Cell Reports
Medicine

Article

Bioengineered human tissue regeneration and repair using endogenous stem cells

Graphical abstract

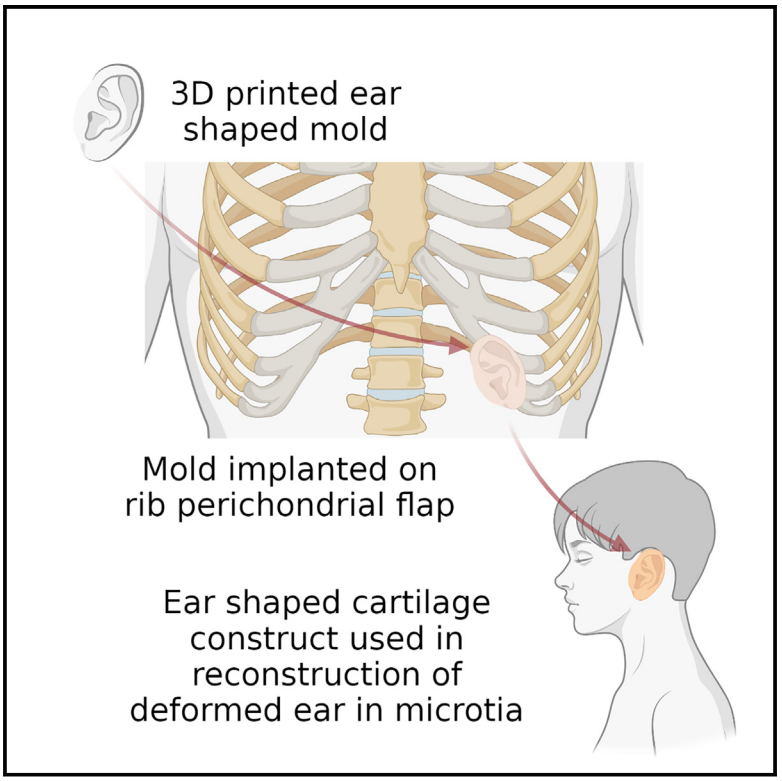

Highlights

- We successfully bioengineered ear and finger joint constructs using patients' own rib space
- These were successfully used to treat unilateral microtia and deformed finger joint
- No exogenous scaffolds were used
- Our results demonstrate the regenerative capability of the ribs

Authors

Jiao Wei, Daniel T. Baptista-Hon, Zi Wang, ..., Lifei Guo, Kang Zhang, Qingfeng Li

Correspondence

lifei.guo@lahey.org (L.G.), kang.zhang@gmail.com (K.Z.), dr.liqingfeng@shsmu.edu.cn (Q.L.)

In brief

Wei et al. develop a method using 3D-printed molds on rib spaces to generate bone and cartilage structures, utilizing the body's own regenerative capabilities. Successful regeneration of finger joints and auricles repaired deformed joints and treated microtia, showing promise for treating bone and tissue defects with good aesthetic and functional outcomes.

Wei et al., 2023, Cell Reports Medicine *4*, 101156
August 15, 2023
https://doi.org/10.1016/j.xcrm.2023.101156

CellPress

Cell Reports Medicine

CellPress
OPEN ACCESS

Article

Bioengineered human tissue regeneration and repair using endogenous stem cells

Jiao Wei,[1,10] Daniel T. Baptista-Hon,[2,3,4,5,10] Zi Wang,[1,10] Gen Li,[4,6,10] Tanja Herrler,[7] Chuanchang Dai,[1] Kai Liu,[1] Baofu Yu,[1] Xiaoxue Chen,[1] Mei Yang,[8] Dong Han,[1] Yuanxu Gao,[2] Ru-Lin Huang,[1,10] Lifei Guo,[9,*] Kang Zhang,[2,3,4,*] and Qingfeng Li[1,11,*]

[1]Department of Plastic and Reconstructive Surgery, Shanghai Ninth People's Hospital, Shanghai Jiao Tong University School of Medicine, Shanghai 200011, China
[2]University Hospital and Center for Biomedicine and Innovations, Faculty of Medicine, Macau University of Science and Technology, Taipa 999078, Macau, China
[3]Zhuhai International Eye Center, Zhuhai People's Hospital and the First Affiliated Hospital of Faculty of Medicine, Macau University of Technology, Zhuhai, Guangdong, China
[4]Department of Bioinformatics and AI, Guangzhou Laboratory, Guangzhou, China
[5]School of Medicine, University of Dundee, Dundee, UK
[6]Guangzhou Women and Children's Medical Center, Guangzhou Medical University, Guangzhou, China
[7]Department of Hand Surgery, Trauma Center Murnau, 82418 Murnau, Germany
[8]Tulane University School of Medicine, New Orleans, LA 70112, USA
[9]Division of Plastic Surgery, Lahey Hospital and Medical Center, Burlington, VT 01808, USA
[10]These authors contributed equally
[11]Lead contact
*Correspondence: lifei.guo@lahey.org (L.G.), kang.zhang@gmail.com (K.Z.), dr.liqingfeng@shsmu.edu.cn (Q.L.)
https://doi.org/10.1016/j.xcrm.2023.101156

SUMMARY

We describe a general approach to produce bone and cartilaginous structures utilizing the self-regenerative capacity of the intercostal rib space to treat a deformed metacarpophalangeal joint and microtia. Anatomically precise 3D molds were positioned on the perichondro-periosteal or perichondral flap of the intercostal rib without any other exogenous elements. We find anatomically precise metacarpal head and auricle constructs within the implanted molds after 6 months. The regenerated metacarpal head was used successfully to surgically repair the deformed metacarpophalangeal joint. Auricle reconstructive surgery in five unilateral microtia patients yielded good aesthetic and functional results. Long-term follow-up revealed the auricle constructs were safe and stable. Single-cell RNA sequencing analysis reveal early infiltration of a cell population consistent with mesenchymal stem cells, followed by IL-8-stimulated differentiation into chondrocytes. Our results demonstrate the repair and regeneration of tissues using only endogenous factors and a viable treatment strategy for bone and tissue structural defects.

INTRODUCTION

Reconstructive surgeries of joint defects through acute or chronic injuries currently rely on the implantation of artificial joints from allogenic donors or from autologous sites.[1–3] However, such approaches are associated with infections and immune rejection. The requirement for low friction between articulating cartilage surfaces in a joint is also difficult to replicate using artificial means, hindering reconstructive joint surgeries.[4] Regenerative medicine using stem cells holds great promise for the treatment of joint defects, but most of the attention has been focused on the use pluripotent stem cells derivatives. There are published attempts of soft tissue engineering of the bladder, esophagus, and cartilage.[5–7] These approaches involve *in vitro* manipulation of bioscaffolds, progenitor cells, and molecular cues. While these are improvements, they are associated with adverse effects such as tumorigenicity and immune rejection.

An attractive alternative is to harness the potential of a patient's endogenous environment for repair and regeneration. Animal studies have demonstrated the generation of new tissues in preformed three-dimensional (3D) scaffolds juxtaposed to areas with a high density of endogenous stem cells, for instance adipose or bone flaps.[8–10] Using this approach, a functional temporomandibular joint osteochondral graft was produced in a subperiosteal chamber in the absence of exogenous stem cells, bioscaffolds, or growth factors in goats.[11,12] We have also previously shown in a swine model that regenerated osteochondral tissue showed physiological and biomechanical properties similar to native tissue.[12] These approaches raise the intriguing possibility that bone structures with cartilaginous components for joint replacement can be produced.[4] There is therefore a potential to extend the current scope of bone regenerative medicine from the treatment of severe fractures to the possibility of regenerating entire bone structures for the treatment of severe bone deformities.

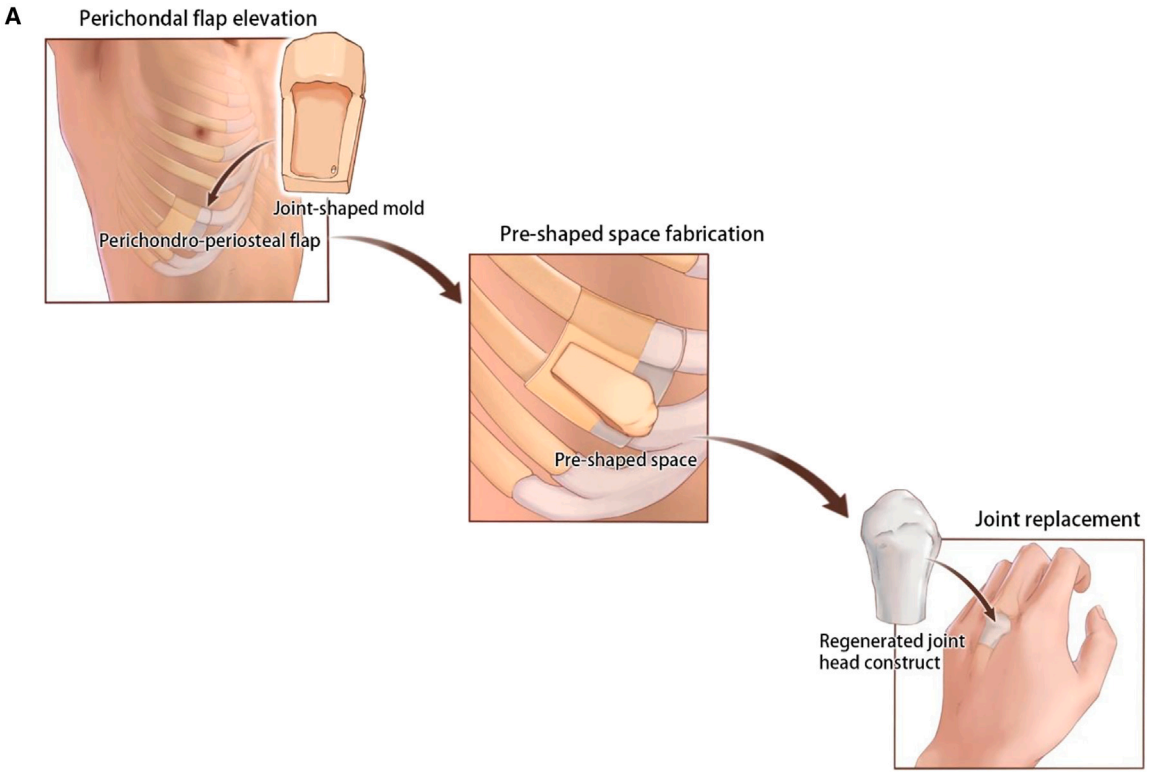

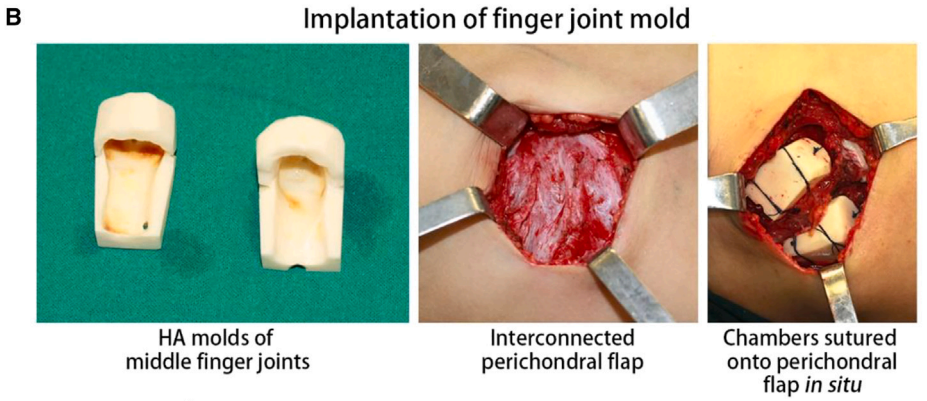

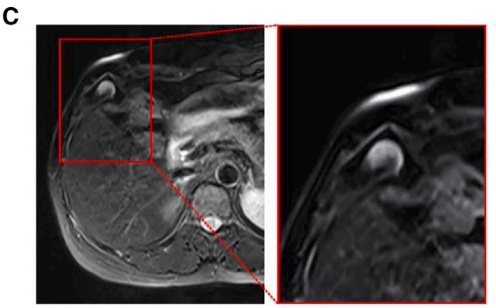

(legend on next page)

In this study, we describe a first-in-human regeneration of a metacarpophalangeal (MP) construct, using a patient's own rib tissue without any exogenous stem cells, bioscaffolds, or growth factors. We used these regenerated joint constructs to replace and repair a severely deformed MP joint. We then tested whether our approach can be used to manufacture anatomically precise ear-shaped cartilaginous constructs in the treatment of five patients with unilateral microtia. We also investigated the gene expression and cell population changes throughout neocartilage regeneration in a swine model of guided cartilage self-regeneration. Our data provide the rationale for a general application for bone and cartilage self-regeneration and represent a paradigm shift in 3D tissue engineering and regenerative medicine.

RESULTS

Reconstruction of a metacarpophalangeal head

Our subject is a 52-year-old woman with a deformed MP joint. She had a long history of restricted and rigid MP joint due to necrosis secondary to trauma-induced ischemia. We hypothesized that the microenvironment within the perichondro-periosteal flap of the intercostal rib would provide the appropriate conditions required to regenerate both the head of the third metacarpal bone and the base of the third proximal phalanx. We obtained CT scans of the subject's healthy contralateral middle finger MP joint and created a 3D digital image of its geometry. A mirror image of this was produced and served as the blueprint to create two finger-shaped models, one for the metacarpal head and the other for the phalanx base. These models were 3D printed and cast in hydroxyapatite (HA), resulting in two finger-shaped molds.

Finger-shaped mold implantation and regeneration of metacarpophalangeal head constructs

The detailed surgical procedure for implantation of the finger-shaped molds into the chest wall is described in the STAR Methods and also summarized in Figure 1A. Briefly, an incision was made on the top of the 6^{th} to 7^{th} ribs, and the periosteum and perichondrium were peeled away from the costal bone and cartilage, respectively. The periosteum and perichondrium were sutured together into an interconnected periosteal-perichondral flap (Figure 1B). The HA molds were then sutured, opening side down and parallel to the cambial surface of the periosteal-perichondral flap. The HA molds were placed at the junctions of the perichondro-periosteal flap from the 6^{th} and 7^{th} intercostal rib of the patient, respectively. MRI scans of the HA molds *in situ* are shown in Figure 1C. 6 months following implantation, the chest wall was opened at the original incision site, and the HA molds were peeled away. Bone-like tissue was found within the chest cavity.

These two MP constructs, one representing the head of the third metacarpal bone and the other for the base of the phalanx, were harvested to repair the patient's necrotic MP joint. During the surgery, it was determined that the tissue necrosis of the patient's original MP joint was limited to the head of the third metacarpal. It was therefore decided that only the regenerated metacarpal head construct will be used for surgery. The unused phalanx base was reserved for histological analyses. The transplanted metacarpal head construct was fixed to the remaining distal portion of middle metacarpal using a narrow titanium plate (Figure 2A). A CT scan revealed appropriate alignment of the transplanted MP head construct (Figure 2B).

We also performed functional analyses of the repaired finger. The extent of flexion of the MP joint was restricted to 5 degrees prior to surgery, highlighting the debilitating nature of our patient's disability. The repaired finger was able to flex up to 42 degrees, indicating a substantial improvement in function (Figure 2C). We also tested the grip strength of the repaired finger. Prior to surgery, the grip strength (kg) in the damaged finger joint was 2.7 kg, compared to 12.3 kg on the contralateral healthy finger joint. Following reconstruction, the grip strength increased to 7.3 kg (compared with 11.3 kg) on the contralateral healthy finger joint. This represents a 2.7-fold improvement in grip strength.

The unused regenerated proximal phalanx base was used for histological analyses. hematoxylin and eosin (H&E) stains of sections of the regenerated phalanx constructs reveal smooth articular cartilage surface connected to subchondral bone. In addition, the distal end of the subchondral bone is characterized by a hollow center filled with bone marrow (Figure 2D). Our study showed a resounding success in the manufacture of cartilage-bone constructs using the patient's own perichondral/periosteal tissue in the treatment of severe joint disabilities.

Auricle reconstruction

Our data reveal that the microenvironment within the perichondro-periosteal flap is conducive for the regeneration of bone and cartilaginous tissue. We tested the generalizability of our approach that cartilaginous tissue alone can be regenerated by using only the microenvironment from the perichondral flap. We tested our approach on five unilateral microtia patients to explore the feasibility and safety of auricular reconstructive surgery, using auricle constructs generated by endogenous stem cells in ear-shaped molds in the absence of other exogenous elements. The study timeline, including the pre-baseline screening, mold design, and fabrication, is summarized in Figure S1.

Between August 2012 and July 2014, we recruited five patients with congenital unilateral microtia (three males and two females, aged between 7 and 16 years; Table S1). All patients

Figure 1. Auricle cartilaginous construct regeneration strategy and timeline

(A) Schematic illustration of MP joint construct fabrication and auricular reconstruction. (1) osteochondral flap was elevated from the 7^{th} to 8^{th} costal cartilage. (2) A finger-shaped HA mold was sutured on the cambial surface of the osteochondral flap to initiate tissue regeneration within the mold. (3) The regenerated joint construct was used for MP joint reconstructive surgery.

(B) Images show (from left to right) the HA molds for the metacarpal head and phalanx base, the elevated and interconnected osteochondral flap in the patient, and the HA molds sutured onto the osteochondral flap *in situ*.

(C) MRI scan of the HA molds *in situ* within the patient's chest cavity.

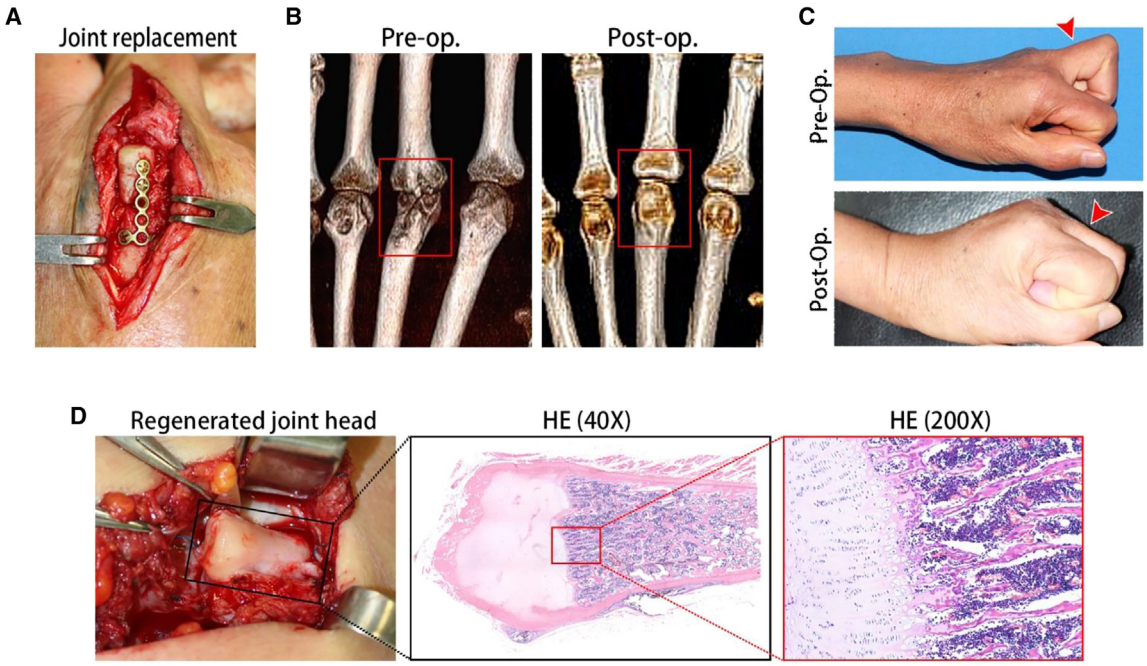

Figure 2. MP regeneration and reconstruction

(A) Transplantation of the head of the third metacarpal construct into the middle finger of the patient. Existing bone is connected to the MP construct using a titanium plate.

(B) CT scan of patient's middle MP joint before and after surgery, demonstrating good alignment of the MP construct.

(C) Functional characterization of the middle finger MP joint. Prior to surgery, the middle finger MP joint was able to flex 5 degrees. Following successful transplantation of the MP construct, the flexion angle was increased to 32 degrees.

(D) The base of the proximal phalanx (not used in the surgery) *in situ* within the chest cavity. H&E stain of sections of the base of the third proximal phalanx shows articular cartilaginous tissue in the head of the bone, fused to subchondral bone characterized by a hollow center filled with bone marrow.

underwent the auricular reconstruction surgeries. Two patients were lost during follow-up. Therefore, three patients were included in our long-term clinical outcomes analysis (mean follow-up period 62 months) to assess the safety of the procedures and stability of the auricular reconstruction construct.

Production and implantation of the ear-shaped mold

The ear-shaped molds were produced based on CT scans of the patients' healthy contralateral ear, similar to the production of the finger-shaped molds above (Figure S2). Briefly, 3D digital images of the healthy contralateral ear were created and served as the blueprint to produce 3D-printed auricle models. These were cast in hydroxyapatite (HA), producing ear-shaped molds. The mold was open on the posterior side of the 3D-printed auricle model and had suturing ports for implantation in the chest wall.

The surgical procedure for auricle HA mold implantation into the chest wall is described in the STAR Methods and also summarized in Figure S3A. Briefly, an incision was made on the top of the 6^{th} to 8^{th} ribs, and the perichondrium was peeled away from the costal cartilage. The 6^{th} to 8^{th} costal cartilages were removed, and the perichondria were sutured together into an interconnected perichondral flap. The ear-shaped HA mold was then sutured, opening side down and parallel to the cambial surface of the perichondral flap. 6–8 months following implantation (mean implantation time 7.2 ± 0.8 months), the chest wall was opened at the original incision site, and the HA molds were peeled away (Figure S3B). In all five patients who underwent the procedure, ear-shaped, cartilage-like tissue was found and explanted (Figure 3).

All five auricle constructs resembled native ears based on overall thickness and the presence of anatomical features (Figure 3A). The auricle constructs were ivory-white in color with a thickness ranging from 2 to 4 mm. They display considerable mechanical strength. All auricle constructs also resembled the patients' healthy ears with specific anatomical features such as a well-defined helix, antihelix, triangular fossa, and cavum conchae.

Histology and physical properties of the regenerated auricular constructs

Following explantation, excess cartilaginous tissues were trimmed from the edges of the auricle constructs (Figure S4A). The trimmed cartilaginous tissues were used for H&E and Alcian blue histological analysis (Figures 3B and 3C, respectively; Table S2). H&E staining is consistent with the presence of chondrocytes (Figure 3B). Alcian blue staining revealed substantial glycosaminoglycans (GAGs) matrices (Figure 3C). Immunohistochemistry, using primary antibodies against collagen type II, revealed the inner matrix in regions positive for GAGs also contained collagen type II (Figure S4B). The outer fibrous tissue was negative for collagen type II. We applied the O'Driscoll histological scoring system[13] on these trimmed regenerated

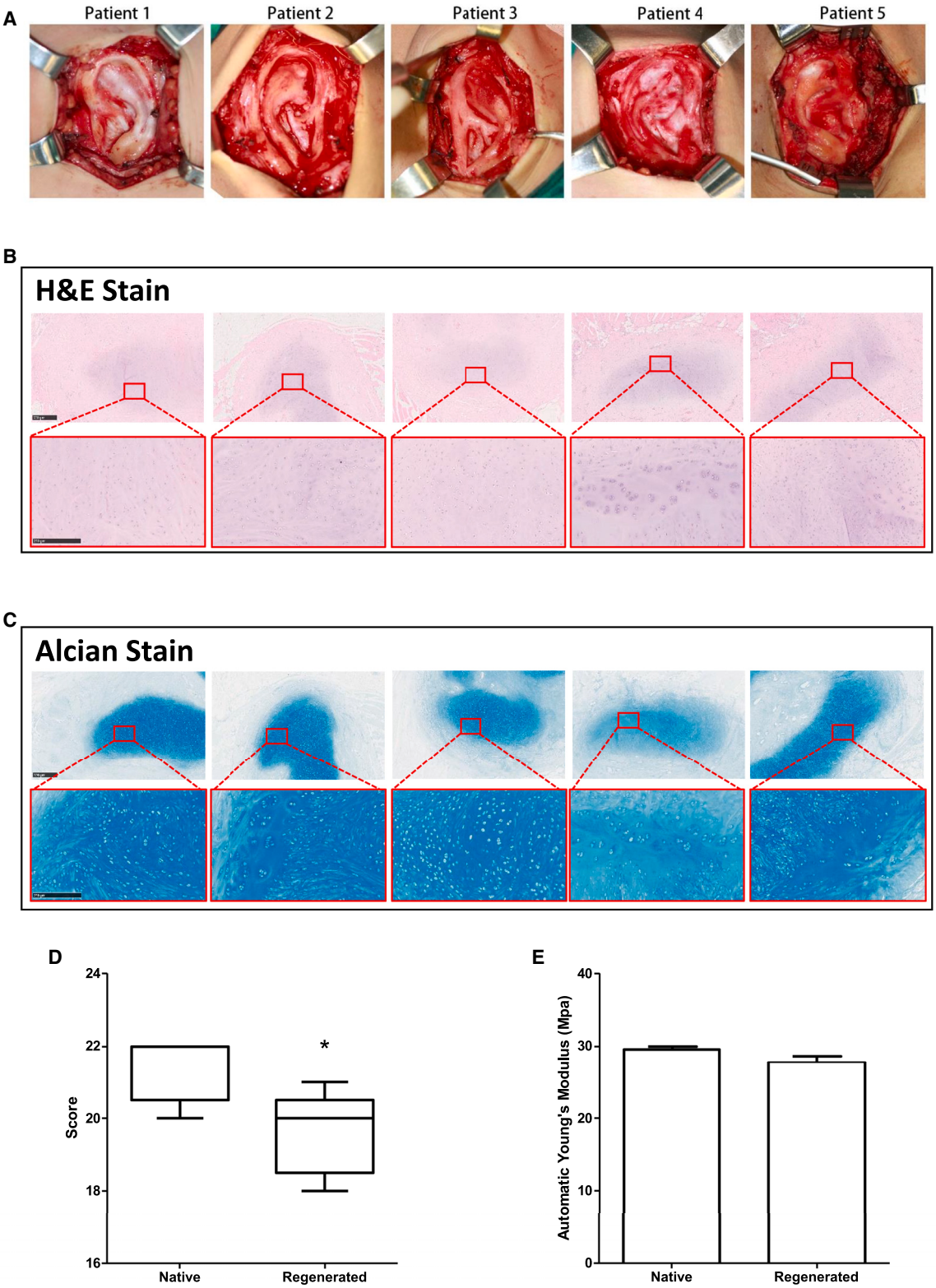

Figure 3. Auricle cartilaginous constructs

(A–C) Images (A) show ear-shaped cartilaginous constructs in patient chest wall 6 to 8 months following implantation of the HA mold. Images are taken following removal of the mold. H&E (B) and Alcian blue (C) histological analysis of excess cartilage trimmed from regenerated cartilaginous constructs prior to surgery.

(legend continued on next page)

cartilaginous tissues and compared them to native cartilage samples (Figure 3D). This scoring system included a number of different grading parameters that take into account cell morphology, matrix staining, structural integrity, and cellularity, which could be used to evaluate the osteochondral junction, clustering and distribution, and adjacent cartilage. This score was used to quantitatively evaluate the extent of cartilage repair based on the criteria of predominant tissue type, structural properties, freedom from degenerative changes in the neighboring cartilage, and freedom from cellular changes of degeneration. The median histological score for native cartilages was 22 (range: 20–22, n = 5), while the median for the regenerated cartilage was 20 (range: 18–21, n = 5). A Mann-Whitney U-test revealed a statistically significant difference ($p = 0.041$), suggesting that the regenerated cartilage showed a small degree of incomplete repair. We also measured the modulus of elasticity of the regenerated cartilage and compared this to native cartilage. The mean (±SEM) of the automatic Young's modulus is shown in Figure 3E. A t test revealed no significant difference in the Young's modulus, indicating that the elasticity of regenerated cartilage is similar to native cartilage.

Auricular reconstruction with the fabricated construct

We used the auricle constructs in auricular reconstructive surgery, adopting Nagata's two-stage technique,[14] which initially involves the implantation of the auricle constructs, followed by construct elevation (Figure S3C). The auricle construct was implanted subcutaneously into the retroarticular region and positioned. Two negative-pressure drainage tubes were placed in the reconstructed ear, one beneath the anterior side of the skin flap and the other beneath the posterior side of the auricle construct. We applied suction to remove the fluid between the auricular construct and skin flap, resulting in a tight attachment of the skin flap onto the auricular construct.

Six months after implantation, the auricle construct was elevated and fixed to the mastoid surface to create an appropriate cephaloauricular angle. The postauricular surface of the reconstructed ear was wrapped in the retroauricular fascial flap. Subsequently, the postauricular surface of the fascia-covered construct was covered with a full-thickness skin graft taken from the hypogastric area of the patient.

We performed further histological analyses on the auricle constructs following auricular reconstructive surgery, by taking a 3-mm biopsy sample from the tragus region with a tissue punch. All five implanted auricle constructs maintained the typical cartilage structure shown above. Two of these examples are shown with the abundant lacuna structure and GAG deposition revealed using Alcian blue staining (Figure S4C and Table S2). Similarly, immunohistochemistry revealed the inner matrix contained collagen type II. Our data indicate that the auricle constructs were histologically stable 6 months post transplantation.

6 months after the elevation surgery, further aesthetic refinement of the reconstructed ear was performed. This included subunit reconstruction, scar removal, and skin flap defatting. Four patients underwent the refinement surgery. One patient did not respond to our follow-up calls and was therefore lost to follow-up at this stage.

Clinical results of the reconstructed ear

We followed up with our patients at 12 months and at least 60 months after refinement surgeries, as outlined in our study plan (Figure S1A). The pre-operative condition of two of the patients and the extent of their microtia are shown in Figure 4A, while the 12-month and long-term follow-up results are shown in Figures 4B and 4C, respectively. One further patient was lost to follow-up 12 months after refinement surgery. In all three patients available for follow-up, their skin grafts were tightly and smoothly attached to the auricle constructs. The aesthetics and geometry of the reconstructed ears displayed the essential anatomical features and appeared symmetrical to the contralateral healthy ear. The skin graft became thinner, and the flexibility of the reconstructed ears improved. Moreover, the helix, cavum conchae, and triangular fossa were also distinct and symmetrical to the shape and size of the healthy contralateral ear. The follow-up results of the three patients are summarized in Table S3. None of the patients required additional refinement surgeries.

Safety assessment

Safety assessment was conducted by patient reports of adverse events following implantation of the HA mold and also following auricular reconstructive surgery. No severe adverse events, such as chest pain, pneumothorax, hematoma, chest wall abnormality, and breathing-related problems, were recorded following HA mold implantation in the chest wall. One patient reported foreign body sensation during strenuous activity while the mold was implanted in the chest cavity. Similarly, no severe adverse events were recorded following the auricular reconstructive surgeries, such as infection, skin graft necrosis, and construct extrusion or deformation. Minor adverse events related to hypertrophic scarring on the posterior side of the reconstructed ears were reported in the first 6 months following construct elevation surgery. These were corrected by further scar revision surgery.

Swine chondrogenesis model

Our study above indicates that anatomically accurate HA molds can be placed on the periosteum and/or perichondrium to produce anatomically accurate bone, cartilaginous, and joint structures, which can be used to correct severe joint defects or microtia. We investigated the cells involved and the genetic changes throughout cartilage self-regeneration in a swine model. Similar to our human studies above, we surgically separated the perichondrium and sutured them together to create a sealed space in 4- to 5-month-old *Sus scrofa*. We recovered tissue from these animals for H&E and Masson staining and analyses at 1 day, 3 days, 7 days, 1 month, 3 months, and 6 months following

(D) Boxplot of histological grading of native and regenerated cartilage. The boxplot was constructed using median (line), interquartile range (box), and minimum/maximum (error bars). A Mann-Whitney U-test found a statistically significant reduction in the histological score in the regenerated cartilage ($p = 0.041$, $n = 5$).
(E) Graph shows mean (±SEM) of the modulus of elasticity for regenerated cartilage versus native cartilage. There was no statistically significant difference in elasticity ($p = 0.094$, t test).

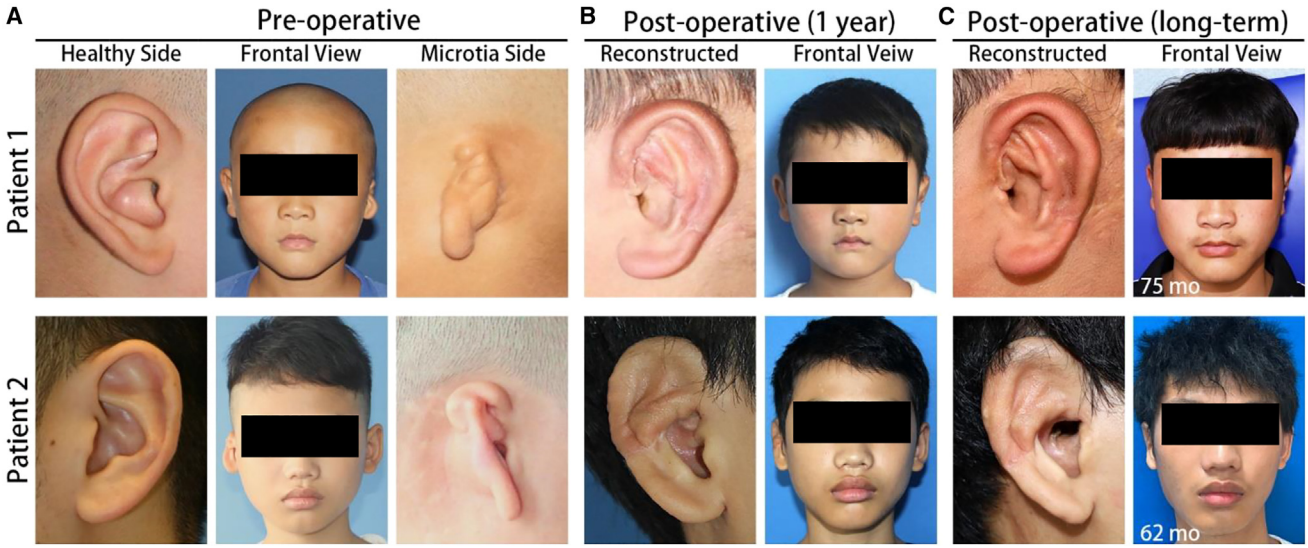

Figure 4. Clinical outcomes of the reconstructed ears in patients 1 and 2

(A) Pre-operative images of the healthy ears, microtia ears, and the frontal view of two of the participants in this study.

(B) 12-month post-operative images of the reconstructed ears and the frontal view of the patients.

(C) Post-operative images of the reconstructed ears and the frontal view of the patients at the last follow-up.

surgery (Figure 5A). We found infiltration of mesenchymal-like cells into the sealed space 3 days after surgery (Figure 5A). These cells possess a fibroblast-like appearance. After 1 week, these cells began to aggregate and appear less differentiated. Cartilage tissue was observed after 1 month, characterized by chondrocytes embedded in a basophilic cartilage matrix. These changes were not seen on the contralateral rib, which did not undergo the surgery (data not shown).

We also measured the elasticity of the recovered cartilage tissues at 1, 3, and 6 months. The modulus of elasticity was normalized to cartilage recovered from the contralateral rib (Figure 5B). We found that the elasticity of the regenerated cartilage was around 65% of control after 1 month. This increased to around 85% after 3 months and close to 100% after 6 months. The increase in elasticity, compared to 1 month, was statistically significant. Our experiments showed that chondrogenesis using a perichondral space can be replicated in a swine model.

Identification of cell populations during cartilage regeneration

Based on the histological analyses above showing that differentiation occurs between 3 and 7 days following surgery in the swine model, we extracted cells from the perichondrium from these two time points and subjected them to single-cell RNA sequencing. The cells from both time points cluster into 19 populations (Figure S5A). Separation of these cells shows that the control perichondrium showed little difference between 3 and 7 days, as would be expected. Interestingly, the cell clustering from the experimental perichondrium recovered 7 days after surgery more resembled that of the control group (Figure S5B). This indicates that the cells in the experimental perichondrium gradually tend to mature normal perichondrium during the regeneration process.

To explore the cells involved in chondrogenesis, we removed endothelial cells, immune cells (macrophages, monocytes, and neutrophils), smooth muscle cells, and myoblasts according to their distinct cell markers (Figures S6A–S6E). We re-clustered the remaining cells, which revealed 13 distinct populations (Figure S7). Within these populations, we found cells expressing markers consistent with fibroblasts (DCN, MFAP5, COL14A1; Figure S8), chondrocytes (COL2A1, COL9A, COL11A; Figure S9), and mesenchymal stem cells (MSCs) (CD106 [VCAM1], CD90 [THY1], CD105 [ENG], and CD73 [NT5E]; Figure S10). Gene expression analysis showed that populations consistent with MSCs (subpopulation 5 and 10) were the main cell type found on day 3, while those consistent with chondrocytes could be identified on day 7 (subpopulations 9 and 12) (Figure S11). Furthermore, consistent with our observation that MSCs could be found on day 3, cells isolated from the regenerated perichondrium at this time point could be differentiated into adipose, bone, and cartilage tissues *in vitro* (Figure S12). These data suggest a differentiation process involving MSCs to chondrocytes from day 3 to day 7.

Genetic and functional analysis of cell clusters responsible for chondrogenesis

Next, we focused on the dynamic cellular changes during chondrogenesis. After removing unrelated cells (subpopulations 2 and 11) (Figure S13), the chronological pseudo-temporal evolution was investigated. Results reveal that the developmental path of the cells begins with C4, C5, and C10 and subsequently C3 and C9 (Figure S14). The expression of stem cell markers CD106, CD105, and CD73 were all enriched at the root of the pseudo-temporal trajectory and gradually decreased along the path, while the expression of differentiated chondrocyte markers COL2A1, COL9A1, and COL11A1 showed exactly the

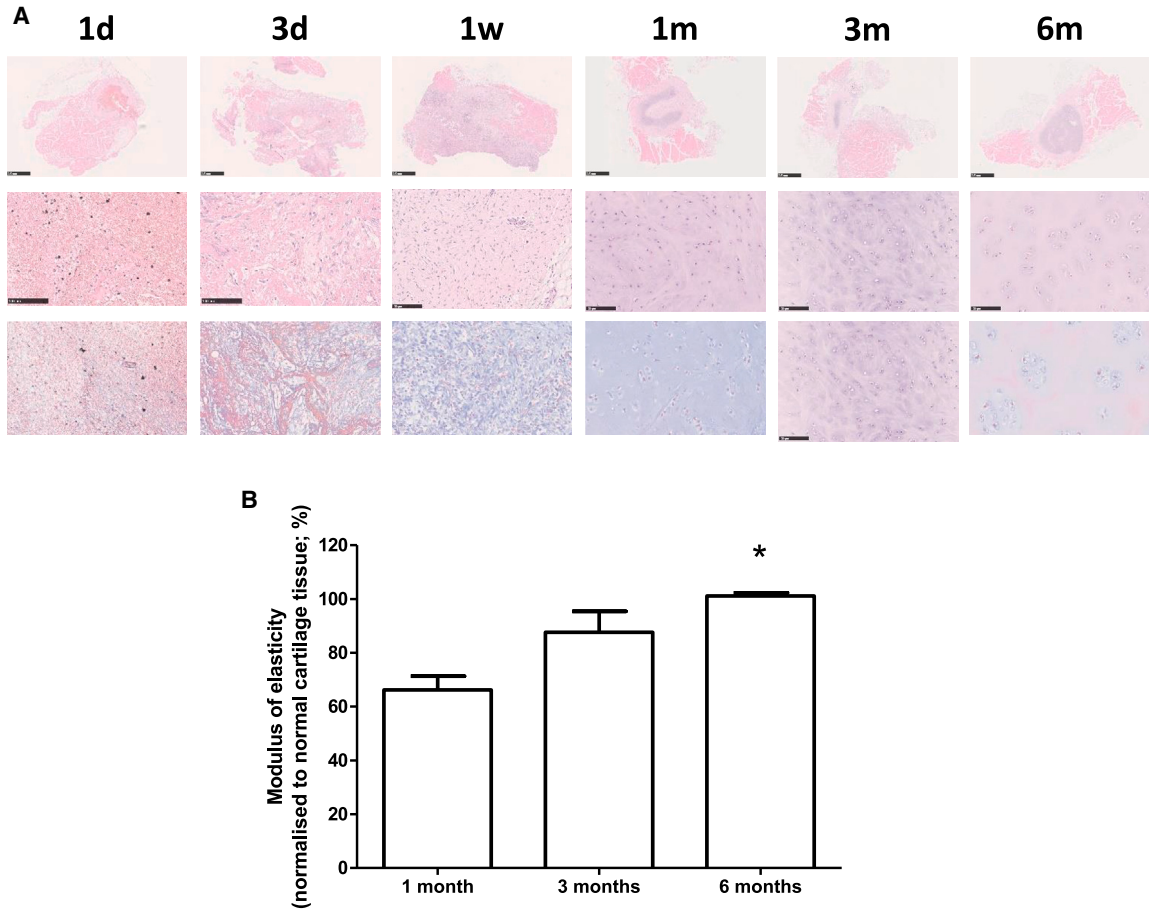

Figure 5. Swine chondrogenesis model

(A) H&E staining of perichondrium and neo-tissue between 1 day and 6 months. Middle panel shows enlarged area indicated by the box. Bottom panel is Masson staining of the same area marked by the box. Scale bars: 100 μm.

(B) Elasticity of the recovered cartilaginous tissue at 1, 3, and 6 months. Graph shows mean (±SEM) of the modulus of elasticity, normalized to that of the contralateral control cartilage tissue. There was a statistically significant increase in the modulus of elasticity between 6 months and 1 month (one-way ANOVA $p = 0.011$; *post hoc* Bonferroni's comparison between 1 month and 6 months $p < 0.05$). It is also noteworthy that the normalized modulus of elasticity at 6 months is close to 100%.

opposite trend as expected. Subpopulation C10 expressed THY1, CD105, CD73, VCAM1, and ITGA11, consistent with MSCs. However, while subpopulations C4 and C5 also co-expressed THY1, CD105, and CD73, only C4 expressed VCAM1, and C5 expressed ITGA11 (Figure S8). Our data also suggest that C5 is more fibrotic than C4 (Figure S8), but C4 expresses chondrocyte markers such as COL2A1 (Figure S9). Interestingly, C5 also expressed markers consistent with proliferating cells (e.g., BIRC5, CENPU, STMN1, CDK1) (Figure S15). These data suggest that C4 may be a group of cells with a differentiation tendency toward chondrogenic progenitor cells (CPCs), while C5 may be a group of proliferating MSC-like cells that appeared on day 3 to regenerate the defective rib cartilage.

In addition, the Sox-trio-positive and COL2A1-positive subpopulations (C8, C9, and C12) can be recognized as chondrocyte lineage. Based on the expression levels of COL2A1, C8 may be premature chondrocytes, while C9 and C12 may be more mature chondrocytes. Interestingly, RUNX2 is absent in C9, suggesting that C9 may be permanent rib chondrocytes, while C12 and C8 may undergo further ossification.

Given population C10 is consistent with MSCs, and C4 may be a group of cells tending toward CPCs that appeared on day 7, we therefore compared the differential expression genes (DEGs) between these two groups. Notably, two immune response-related genes, interleukin-8 (IL1B) and CXCL8, expressed higher in C10 (Figure S16), which suggested critical roles of these two factors in early healing response. The highly differentially expressed collagen genes in C4 further implied its differentiation tendency as CPCs (Figure S16). Consistent with this observation, we found an increase in IL-8 expression in the perichondrium at day 3, and exposure of perichondrial cells *in vitro* to IL-8 stimulated the expression of collagen II as well as the chondrocyte transcription factor SOX9 (Figure S17).

Our data suggest that guided endogenous cartilage regeneration can be divided into distinct phases (Figure 6). Following the surgical insult to the perichondrium/periosteum, an immune

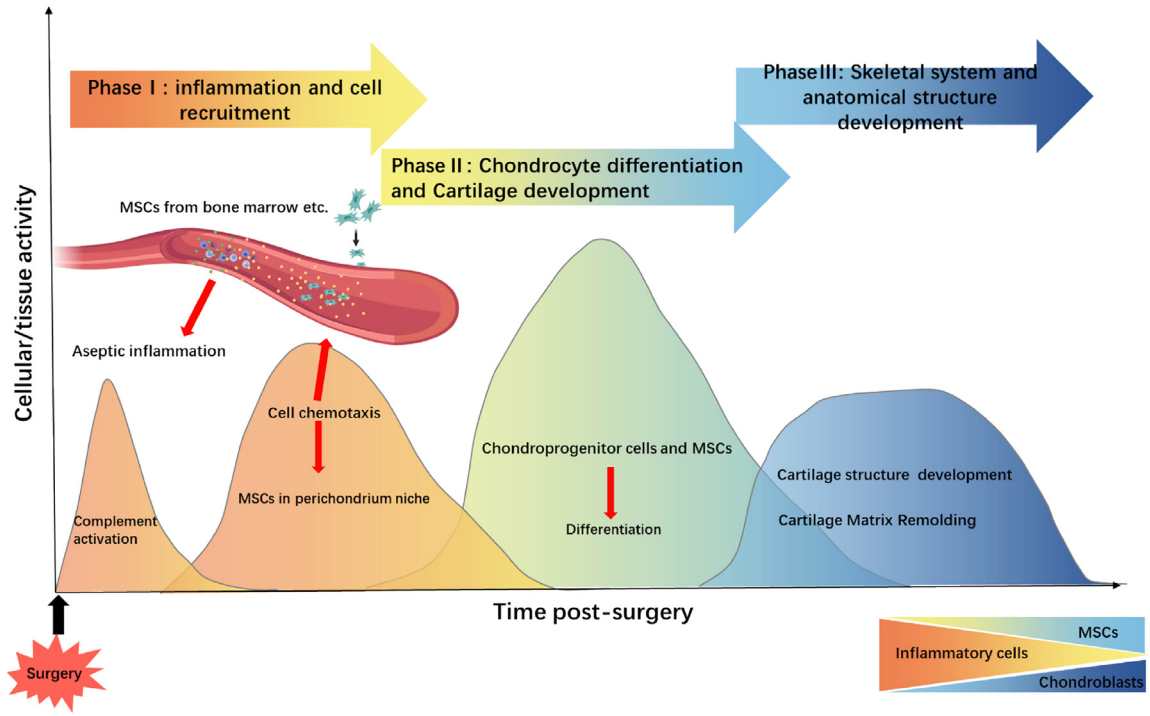

Figure 6. Model of cartilage self-regeneration

Our data suggest that guided endogenous cartilage regeneration involved an initiation of inflammation and recruitment of immune cells, followed by recruitment of mesenchymal stem cells into the engineered space. These then differentiate into proliferating chondrogenic progenitor cells and ultimately chondrocytes, which lay down the extracellular matrices consistent with cartilage tissue.

response characterized by complement activation and immune cell infiltration ensues, leading to an inflammatory response. Our functional data indicate that an increase in IL1B and CXCL8 mediates the early healing response. Our single-cell RNA sequencing data indicate the presence of MSCs in the regenerating tissue after 3 days. These, together with increased IL-8, may be involved in the increased number of proliferating chondrogenic precursor cells, followed by chondrocytes, which lay down the extracellular matrices consistent with cartilage tissue.

DISCUSSION

Stem cell therapy holds great promise in regenerative medicine, and the repair and regeneration of tissues for therapeutic purposes remains an ultimate goal. So far, most efforts have focused on the use of pluripotent stem cells and their derivatives. This is not an ideal approach, not the least because of the potential of immune rejection and tumorigenicity. One attractive alternative is to use endogenous stem cells in the regeneration of damaged tissues. Promising results have been demonstrated in the treatment of eye disorders, where preservation of lens epithelial stem cells allows for functional lens regeneration following cataract removal.[15] Endogenous stem cells in the retina can also be reprogrammed to produce retinal precursors and photoreceptors, offering the possibility of retinal regeneration.[16] For joint regeneration, promising results have also been achieved in rabbit using bioscaffolds infused with growth-factor adsorbed hydrogels.[17] These approaches highlight the enormous potential of endogenous stem cells in regenerative medicine.[18,19]

However, the approaches that harness the potential of endogenous stem cells involve, to some extent, *in vitro* manipulation of bioscaffolds, progenitor cells, and molecular cues.[20] These are associated with tumorigenicity and potential immune rejection. The ideal approach is to manufacture tissue constructs within the patient's body, free of any exogenous elements. The rib has a remarkable ability to regenerate itself, dependent on the perichondrium and periosteum. These are fibrous sheaths of vascular connective tissue that surround the rib cartilage and bone, respectively. A number of studies, including from our group, suggest that costal cartilage and bone are capable of regeneration, provided the perichondrium and periosteum are intact.[12,21–24] This has proved successful to mold mandibular-shaped bone or S-shaped cartilage tissue in animal models.[25,26] In this study, we achieved a first-in-human approach to regenerate MP joint constructs for the treatment of severe joint deformity. Using the same approach, we also successfully manufactured precise auricle cartilaginous constructs to treat five unilateral microtia patients.

Indeed, we were able to demonstrate for the first time the regeneration of middle finger MP head and phalanx bone constructs using the costochondral junction. The construct displayed a combination of both bone and cartilage segments and was used successfully to reconstruct the patient's severely deformed middle finger joint. We were able to demonstrate

excellent post-surgical alignment of the joint and also an improvement in the degree of flexion as well as grip strength.

We reasoned that our approach can be extended to manufacture pure cartilaginous constructs, by using only the perichondral section of the rib. Auricle reconstruction following trauma, tumors, or congenital deformities remains one of the more challenging tasks in reconstructive surgery, in which the engineering of an anatomically suitable cartilaginous auricle is a prerequisite.[27,28] Auricle constructs fabricated using multiple manually carved autologous costal cartilage or high-density porous polyethylene materials have been used clinically.[29–31] These fabricated auricle constructs are associated with a number of drawbacks. These include the removal of 2–3 ribs leading to injury at the harvesting site, instability and resultant deformity of the auricle construct, and finally a stringent skill requirement for manually carving the construct, leading to large variations in clinical outcomes.[29–31] We used CT scanning coupled with 3D printing to ensure that the HA molds had detailed, patient-specific anatomical features modeled on the patients' healthy contralateral ear.[20] These constructs were successfully used in auricular reconstructive surgery in three microtia patients. These auricle constructs displayed considerable mechanical strength and in our long-term follow-up withstood the compressive pressures of the skin. The reconstructed ears were also stable in the long term, and there were no severe adverse effects.

The regenerative capacity of the perichondrium and periosteum may lie in its provision of a rich *in vivo* microenvironment with vascular supply and stem cell niche within which endogenous stem cells reside. These are required for the production of chondrocytes and osteocytes, respectively, for cartilage and bone regeneration. Tissue regeneration within the HA mold first requires the endogenous stem cell population in the perichondrium and periosteum to differentiate and migrate into the space created by the mold. Our single-cell RNA sequencing data show that cells consistent with MSCs were found within the engineered tissue regeneration space from as early as 3 days post surgery. While whether this MSC-like subpopulation is indeed a bona fide endogenous stem cell population is not clear, our data show that cells extracted at this time point could be induced *in vitro* to differentiate into different cell types, including chondrocytes. This may reflect a direct mechanism for the involvement of these MSC-like cells in bone and cartilage regeneration, through differentiation into proliferating chondrocytes. However, it is also possible that other bona fide stem cells, such as skeletal stem cells (SSCs), might be involved. SSCs are a source of cells for bone development, homeostasis, and injury repair[32,33] and are likely to be present in the periosteum.[34] The MSC-like cell population identified in our study may have chondrogenically or osteogenically committed progenitor cells that migrate into the HA mold and create an environment required for SSCs to differentiate into osteocytes or chondrocytes. The release of IL-8 due to the inflammation caused by the trauma of the surgery, incision of the perichondrium/periosteum, as well as implantation of the mold may play a critical role in stimulating the differentiation of MSCs into proliferating CPCs. Indeed, we show that *in vitro* treatment of extracted perichondrial cells with IL-8 stimulated the expression of SOX9, which is a chondrocyte transcription factor.[35] IL-8 also acts as a chemoattractant for a variety of cells, including neutrophils. There may be an important role played by neutrophils in bone regeneration, which may orchestrate the infiltration of endogenous stem cells (such as SSCs) and adaptive immune cells during the early stages of bone healing and regeneration.[36] This may initiate a tissue healing and remodeling process akin to native rib regeneration.[24] Remodeling within the HA mold will require cell migration from the perichondral/periosteal flap into the empty space. Deposition of extracellular matrix (ECM) proteins within the HA mold is likely to be a prerequisite for tissue regeneration. For example, meniscus-derived ECM promotes the infiltration of meniscal stem cells into a scaffold.[37] The fluid-tissue interface at the leading edge of cell infiltration might generate increased surface tension on the cells, which might impact the morphogenesis process.[38–40] We found cell populations consistent with fibroblasts within the regenerating tissue during the early stages of regeneration. These fibroblasts express COL14A1, which has been suggested to play a regulatory role in early stages of collagen fibrillogenesis.[41] These processes may guide the infiltration of MSCs into the HA mold, which are then stimulated to differentiate into chondrocytes through the actions of IL-8.

Our study demonstrated no severe adverse events following implantation of the HA mold into the chest cavity. HA has been extensively used in different clinical settings including bony morphogenesis applications and has a good safety profile. The influence of the biomaterial used to fabricate the mold on the regeneration of cartilaginous or bone tissues will be an important area of research. Numerous biomaterials with different properties exist.[18]

In summary, this study established a novel and paradigm-shifting method in structural regenerative medicine. We were able to generate functional and clinically applicable cartilaginous and bone constructs for auricular and joint reconstructive surgeries. The results of our study have laid the basis for larger clinical studies in other small bone or cartilage defects (e.g., temporomandibular joints and nasal cartilage). Our study also raises the interesting possibility of correcting small bone and cartilage defects in children. However, we emphasize that the size of the regenerated tissue will be limited by the restricted area of the costal perichondrium in children. Our study also presented intriguing insights into "space-induced regeneration" and raises the possibility of similar approaches for regeneration in other organs, particularly those with complex structures and geometries. Importantly, the approach used in this study will drastically reduce outcome variation dependent on individual surgeon experience. We therefore anticipate that our approach and results will be reliably reproducible in larger studies.

Limitations of the study

While the clinical results of our proof-of-concept study were favorable, the study has a number of weaknesses, including the relatively small sample size, which precluded meaningful statistical analyses. Nevertheless, the biomechanical and histological properties of regenerated and native cartilages were comparable. In comparison with other approaches described above, our method requires an additional surgery to implant the mold into the patients, which comes with additional risks. While the aesthetics of the regenerated auricular and finger constructs

were good, regeneration required 6 months, which may not be an issue with congenital deformities such as microtia but may be lengthy for the repair of small bone deformities from acute trauma. Finally, the cartilage produced using the ribs is hyaline cartilage, while endogenous ear cartilage is elastic. There will be differences in elasticity, but our clinical results showed that the aesthetic outcomes were good, and the reconstructed outer ears were stable.

STAR★METHODS

Detailed methods are provided in the online version of this paper and include the following:

- KEY RESOURCES TABLE
- RESOURCE AVAILABILITY
  - Lead contact
  - Materials availability
  - Data and code availability
- EXPERIMENTAL MODEL AND SUBJECT DETAILS
  - Auricular reconstruction study design
  - Metacarpophalangeal joint reconstruction study design
  - Porcine model and surgical procedure
- METHOD DETAILS
  - Clinical study follow-up and assessment of clinical outcome
  - Ear and finger-shaped chamber fabrication
  - Metacarpophalangeal joint bones construct regeneration
  - Auricle construct regeneration
  - Metacarpophalangeal joint reconstructive surgery
  - Auricular reconstructive surgery
  - Histology analysis
  - Immunoblotting
  - RNA extraction
  - Single cell RNA sequencing
  - Statistical analysis

SUPPLEMENTAL INFORMATION

Supplemental information can be found online at https://doi.org/10.1016/j.xcrm.2023.101156.

ACKNOWLEDGMENTS

This research was supported by grants from the Shanghai Municipal Key Clinical Specialty (grant no. shslczdzk00901), the National Natural Science Foundation of China (grant nos. 81871571, 81871572, 81702727), and Macau Science and Technology Development Fund, Macao (0007/2020/AFJ, 0070/2020/A2, 0109/2020/A3, 0003/2021/AKP). We would also like to thank Dr Hong Ouyang for expert discussions on single cell RNA sequencing results.

AUTHOR CONTRIBUTIONS

J.W., D. T. B-H., Z.W., G.L., R-L.H., T.H., C.D., K.L., B.Y., X.C., M.Y., D.H., Y.G., L.G., K.Z. and Q.L. collected and/or analyzed the data. K.Z. and Q.L. conceived and supervised the project. K.Z., Q.L., J.W., D. T. B-H., Z.W., G.L., and R-L.H. wrote and/or revised the manuscript. All authors discussed the results and reviewed the manuscript.

DECLARATION OF INTERESTS

The authors declare no competing interests.

Received: October 18, 2022
Revised: April 30, 2023
Accepted: July 19, 2023
Published: August 15, 2023

REFERENCES

1. Brooks, P.M. (2006). The burden of musculoskeletal disease–a global perspective. Clin. Rheumatol. *25*, 778–781.
2. Lawrence, R.C., Felson, D.T., Helmick, C.G., Arnold, L.M., Choi, H., Deyo, R.A., Gabriel, S., Hirsch, R., Hochberg, M.C., Hunder, G.G., et al. (2008). Estimates of the prevalence of arthritis and other rheumatic conditions in the United States. Part II. Arthritis Rheum. *58*, 26–35.
3. Helmick, C.G., Felson, D.T., Lawrence, R.C., Gabriel, S., Hirsch, R., Kwoh, C.K., Liang, M.H., Kremers, H.M., Mayes, M.D., Merkel, P.A., et al. (2008). Estimates of the prevalence of arthritis and other rheumatic conditions in the United States. Part I. Arthritis Rheum. *58*, 15–25.
4. Klein, J. (2009). Chemistry. Repair or replacement–a joint perspective. Science *323*, 47–48.
5. Atala, A., Bauer, S.B., Soker, S., Yoo, J.J., and Retik, A.B. (2006). Tissue-engineered autologous bladders for patients needing cystoplasty. Lancet *367*, 1241–1246.
6. Dua, K.S., Hogan, W.J., Aadam, A.A., and Gasparri, M. (2016). In-vivo oesophageal regeneration in a human being by use of a non-biological scaffold and extracellular matrix. Lancet *388*, 55–61.
7. Fulco, I., Miot, S., Haug, M.D., Barbero, A., Wixmerten, A., Feliciano, S., Wolf, F., Jundt, G., Marsano, A., Farhadi, J., et al. (2014). Engineered autologous cartilage tissue for nasal reconstruction after tumour resection: an observational first-in-human trial. Lancet *384*, 337–346.
8. Dolderer, J.H., Abberton, K.M., Thompson, E.W., Slavin, J.L., Stevens, G.W., Penington, A.J., and Morrison, W.A. (2007). Spontaneous large volume adipose tissue generation from a vascularized pedicled fat flap inside a chamber space. Tissue Eng. *13*, 673–681.
9. Findlay, M.W., Dolderer, J.H., Trost, N., Craft, R.O., Cao, Y., Cooper-White, J., Stevens, G., and Morrison, W.A. (2011). Tissue-engineered breast reconstruction: bridging the gap toward large-volume tissue engineering in humans. Plast. Reconstr. Surg. *128*, 1206–1215.
10. Stevens, M.M., Marini, R.P., Schaefer, D., Aronson, J., Langer, R., and Shastri, V.P. (2005). In vivo engineering of organs: the bone bioreactor. Proc. Natl. Acad. Sci. USA *102*, 11450–11455.
11. Wei, J., Herrler, T., Han, D., Liu, K., Huang, R., Guba, M., Dai, C., and Li, Q. (2016). Autologous temporomandibular joint reconstruction independent of exogenous additives: a proof-of-concept study for guided self-generation. Sci. Rep. *6*, 37904.
12. Wei, J., Herrler, T., Liu, K., Han, D., Yang, M., Dai, C., and Li, Q. (2016). The Role of Cell Seeding, Bioscaffolds, and the In Vivo Microenvironment in the Guided Generation of Osteochondral Composite Tissue. Tissue Eng. *22*, 1337–1347.
13. O'Driscoll, S.W., Keeley, F.W., and Salter, R.B. (1986). The chondrogenic potential of free autogenous periosteal grafts for biological resurfacing of major full-thickness defects in joint surfaces under the influence of continuous passive motion. An experimental investigation in the rabbit. J. Bone Joint Surg. Am. *68*, 1017–1035.
14. Nagata, S. (1993). A new method of total reconstruction of the auricle for microtia. Plast. Reconstr. Surg. *92*, 187–201.
15. Lin, H., Ouyang, H., Zhu, J., Huang, S., Liu, Z., Chen, S., Cao, G., Li, G., Signer, R.A.J., Xu, Y., et al. (2016). Lens regeneration using endogenous stem cells with gain of visual function. Nature *531*, 323–328.
16. Zhao, J.J., Ouyang, H., Luo, J., Patel, S., Xue, Y., Quach, J., Sfeir, N., Zhang, M., Fu, X., Ding, S., et al. (2014). Induction of retinal progenitors

and neurons from mammalian Müller glia under defined conditions. J. Biol. Chem. *289*, 11945–11951.

17. Lee, C.H., Cook, J.L., Mendelson, A., Moioli, E.K., Yao, H., and Mao, J.J. (2010). Regeneration of the articular surface of the rabbit synovial joint by cell homing: a proof of concept study. Lancet *376*, 440–448.
18. Xia, H., Li, X., Gao, W., Fu, X., Fang, R.H., Zhang, L., and Zhang, K. (2018). Tissue repair and regeneration with endogenous stem cells. Nat. Rev. Mater. *3*, 174–193.
19. Stern, J.H., Tian, Y., Funderburgh, J., Pellegrini, G., Zhang, K., Goldberg, J.L., Ali, R.R., Young, M., Xie, Y., and Temple, S. (2018). Regenerating Eye Tissues to Preserve and Restore Vision. Cell Stem Cell *23*, 453–849.
20. Zhou, G., Jiang, H., Yin, Z., Liu, Y., Zhang, Q., Zhang, C., Pan, B., Zhou, J., Zhou, X., Sun, H., et al. (2018). In Vitro Regeneration of Patient-specific Ear-shaped Cartilage and Its First Clinical Application for Auricular Reconstruction. EBioMedicine *28*, 287–302.
21. LESTER, C.W. (1959). Tissue replacement after subperichondrial resection of costal cartilage: two case reports. Plast. Reconstr. Surg. Transplant. Bull. *23*, 49–54.
22. Chang, P.Y., Lai, J.Y., Chen, J.C., and Wang, C.J. (2006). Long-term changes in bone and cartilage after Ravitch's thoracoplasty: findings from multislice computed tomography with 3-dimensional reconstruction. J. Pediatr. Surg. *41*, 1947–1950.
23. Philip, S.J., Kumar, R.J., and Menon, K.V. (2005). Morphological study of rib regeneration following costectomy in adolescent idiopathic scoliosis. Eur. Spine J. *14*, 772–776.
24. Srour, M.K., Fogel, J.L., Yamaguchi, K.T., Montgomery, A.P., Izuhara, A.K., Misakian, A.L., Lam, S., Lakeland, D.L., Urata, M.M., Lee, J.S., and Mariani, F.V. (2015). Natural large-scale regeneration of rib cartilage in a mouse model. J. Bone Miner. Res. *30*, 297–308.
25. Cheng, M.H., Brey, E.M., Allori, A.C., Gassman, A., Chang, D.W., Patrick, C.W., Jr., and Miller, M.J. (2009). Periosteum-guided prefabrication of vascularized bone of clinical shape and volume. Plast. Reconstr. Surg. *124*, 787–795.
26. Bohdan, P., Baraa, Z., and Yusuf, K. (2007). Guided cartilage regeneration using resorbable template. Eplasty *8*, e5.
27. Xing, W., Kang, C., Wang, Y., and Zhang, Q. (2018). Reconstruction of Microtia Using a Single Expanded Postauricular Flap without Skin Grafting: Experience of 683 Cases. Plast. Reconstr. Surg. *142*, 170–179.
28. Denadai, R., Raposo-Amaral, C.E., Zanco, G.L., and Raposo-Amaral, C.A. (2019). Autologous Ear Reconstruction for Microtia Does Not Result in Loss of Cutaneous Sensitivity. Plast. Reconstr. Surg. *143*, 808e–819e.
29. Xu, Z., Xu, F., Zhang, R., Zhang, Q., Li, D., and Li, Y. (2017). A New Classification of Helix Fabrication Methods with Autogenous Costal Cartilage in Microtia Reconstruction. Plast. Reconstr. Surg. *139*, 1315e–1324e.
30. Reinisch, J., and Tahiri, Y. (2018). Polyethylene Ear Reconstruction: A State-of-the-Art Surgical Journey. Plast. Reconstr. Surg. *141*, 461–470.
31. Reinisch, J.F., van Hövell Tot Westerflier, C.V.A., Tahiri, Y., and Yao, C.A. (2019). The Occipital Artery-Based Fascial Flap for Ear Reconstruction. Plast. Reconstr. Surg. *143*, 592e–601e.
32. Li, Q., Xu, R., Lei, K., and Yuan, Q. (2022). Insights into skeletal stem cells. Bone Res. *10*, 61.
33. Marecic, O., Tevlin, R., McArdle, A., Seo, E.Y., Wearda, T., Duldulao, C., Walmsley, G.G., Nguyen, A., Weissman, I.L., Chan, C.K.F., and Longaker, M.T. (2015). Identification and characterization of an injury-induced skeletal progenitor. Proc. Natl. Acad. Sci. USA *112*, 9920–9925.
34. Duchamp de Lageneste, O., Julien, A., Abou-Khalil, R., Frangi, G., Carvalho, C., Cagnard, N., Cordier, C., Conway, S.J., and Colnot, C. (2018). Periosteum contains skeletal stem cells with high bone regenerative potential controlled by Periostin. Nat. Commun. *9*, 773.
35. Kozhemyakina, E., Lassar, A.B., and Zelzer, E. (2015). A pathway to bone: signaling molecules and transcription factors involved in chondrocyte development and maturation. Development *142*, 817–831.
36. Cai, B., Lin, D., Li, Y., Wang, L., Xie, J., Dai, T., Liu, F., Tang, M., Tian, L., Yuan, Y., et al. (2021). N2-Polarized Neutrophils Guide Bone Mesenchymal Stem Cell Recruitment and Initiate Bone Regeneration: A Missing Piece of the Bone Regeneration Puzzle. Adv. Sci. *8*, e2100584.
37. Ruprecht, J.C., Waanders, T.D., Rowland, C.R., Nishimuta, J.F., Glass, K.A., Stencel, J., DeFrate, L.E., Guilak, F., Weinberg, J.B., and McNulty, A.L. (2019). Meniscus-Derived Matrix Scaffolds Promote the Integrative Repair of Meniscal Defects. Sci. Rep. *9*, 8719.
38. Lecuit, T., and Le Goff, L. (2007). Orchestrating size and shape during morphogenesis. Nature *450*, 189–192.
39. Lecuit, T., and Lenne, P.F. (2007). Cell surface mechanics and the control of cell shape, tissue patterns and morphogenesis. Nat. Rev. Mol. Cell Biol. *8*, 633–644.
40. Manning, M.L., Foty, R.A., Steinberg, M.S., and Schoetz, E.M. (2010). Coaction of intercellular adhesion and cortical tension specifies tissue surface tension. Proc. Natl. Acad. Sci. USA *107*, 12517–12522.
41. Ansorge, H.L., Meng, X., Zhang, G., Veit, G., Sun, M., Klement, J.F., Beason, D.P., Soslowsky, L.J., Koch, M., and Birk, D.E. (2009). Type XIV Collagen Regulates Fibrillogenesis: PREMATURE COLLAGEN FIBRIL GROWTH AND TISSUE DYSFUNCTION IN NULL MICE. J. Biol. Chem. *284*, 8427–8438.
42. Butler, A., Hoffman, P., Smibert, P., Papalexi, E., and Satija, R. (2018). Integrating single-cell transcriptomic data across different conditions, technologies, and species. Nat. Biotechnol. *36*, 411–420.
43. Macosko, E.Z., Basu, A., Satija, R., Nemesh, J., Shekhar, K., Goldman, M., Tirosh, I., Bialas, A.R., Kamitaki, N., Martersteck, E.M., et al. (2015). Highly Parallel Genome-wide Expression Profiling of Individual Cells Using Nanoliter Droplets. Cell *161*, 1202–1214.
44. Aran, D., Looney, A.P., Liu, L., Wu, E., Fong, V., Hsu, A., Chak, S., Naikawadi, R.P., Wolters, P.J., Abate, A.R., et al. (2019). Reference-based analysis of lung single-cell sequencing reveals a transitional profibrotic macrophage. Nat. Immunol. *20*, 163–172.

STAR★METHODS

KEY RESOURCES TABLE

REAGENT or RESOURCE	SOURCE	IDENTIFIER
Antibodies		
Anti-collagen II	Abcam	ab34712; RRID:AB_731688
Anti-CXCL8	USBiological life science	141075
Anti-aggrecan	Abcam	ab3773; RRID:AB_304066
Anti-SOX9	Abcam	ab185966; RRID:AB_2728660
Anti-RPL4	Santa Cruz Biotechnology	sc-100838; RRID:AB_2181910
Secondary HRP antibody	Abcam	ab6759; RRID:AB_955434
Chemicals, peptides, and recombinant proteins		
Mayer's H&E	Beyotime, China	C0105S
Masson stain	Sen Bei Jia Biotech, China	SBJ-0290
Trizol reagent	Invitrogen	15596018
Deposited data		
scRNAseq data - Part 1	Mendeley Data	https://doi.org/10.17632/fxw54hss8r.1
scRNAseq data - Part 2	Mendeley Data	https://doi.org/10.17632/vgwws7ffxb.1
scRNAseq data - Part 3 & 4	Mendeley data	https://doi.org/10.17632/8tgyy2w32r.1
Experimental models: Organisms/strains		
Sus scrofa	Shanghai Jiagan Biotechnology Co., LTD	Bama miniature pig
Software and algorithms		
Origin 8.0	OriginLab, MA, USA	N/A
Cutadapt (v1.15)	https://github.com/marcelm/cutadapt/archive/refs/tags/v1.15.zip	N/A
HISTAT2 v2.0.5	https://github.com/DaehwanKimLab/hisat2/archive/refs/tags/v2.0.5.zip	N/A
Cell Ranger 3.1.0	10x Genomics	N/A
R package Seurat 3.0	https://github.com/satijalab/seurat/archive/refs/tags/v3.0.0.zip	N/A
R package SingleR	https://github.com/dviraran/SingleR/archive/refs/heads/master.zip	N/A
GraphPad Prism 5.2	GraphPad Software, CA, USA	N/A

RESOURCE AVAILABILITY

Lead contact

Further information and requests for resources and reagents should be directed to and will be fulfilled by the lead contact, Qingfeng Li (dr.liqingfeng@shsmu.edu.cn).

Materials availability

This study did not generate new unique reagents.

Data and code availability

Single-cell RNA-seq data have been deposited at Mendeley Data and are publicly available as of the date of publication. The DOI is listed in the key resources table. Microscopy data reported in this paper will be shared by the lead contact upon request. Any additional information required to reanalyze the data reported in this paper is available from the lead contact upon request.

EXPERIMENTAL MODEL AND SUBJECT DETAILS

Auricular reconstruction study design

This is a single-site clinical pilot study. The procedures comply with the principles of the Declaration of Helsinki from the International Conference on Harmonization. Participants were eligible for this study if they had congenital unilateral microtia requiring auricular reconstruction that may not have been treated by other auricular reconstruction surgeries, were older than 6 years of age in which the ear has stopped growing and bust larger than 55 cm, and had no history of systemic disease. Key exclusion criteria included poor state of health, those with blood diseases or bleeding tendencies, women who were pregnant, lactating, or planning to become pregnant within 1 year and those with psychological disorders. Patients with unilateral microtia were recruited to the study after obtaining a written informed consent. The study protocol and the informed consent document were approved by the institutional review board of Shanghai Ninth People's Hospital.

Metacarpophalangeal joint reconstruction study design

This is a clinical pilot study in which a 52-year-old woman with a deformed MP joint was recruited. She had a long history of a restricted and rigid MP joint due to necrosis secondary to trauma-induced ischemia. The patient signed an informed consent. The study protocol and the informed consent document were approved by the institutional review board of Shanghai Ninth People's Hospital.

Porcine model and surgical procedure

We used adult and healthy *Sus scrofa* (n = 19), 4 to 5 months old, of both sexes. The average weight of these laboratory animals was 20.0 ± 2.5 kg. All swine were randomly divided into seven groups (A-G), the first five groups consisted of 3 swine per group while the last two consisted of 2 swine per group. Costal cartilages of each swine were randomly divided into the experimental side and control side. After being housed in relevant facilities under standard conditions for one week, every swine underwent surgical procedures, as described in our previous study.(13) In general, the chondro-osseous junction of the third or fourth rib counting from the tail of the experimental side of each swine was exposed (Figure 1A). The perichondrium was separated from the costal cartilage and a length of 2 cm cartilage was removed (Figures 1B and 1C). Then, 6-0 PDS was used to suture the separated perichondrium, a closed space was created as a sealed sheath (Figure 1D), and the wound was carefully closed.

The costal cartilage and perichondrium of the control side were retained with no procedure performed. The time points of execution were 1day, 3days, 1W, 2W, 1M, 3M, and 6M, corresponding to groups A-G. After sacrifice, the perichondrium of both the experimental and control sides was subjected to histological examination and transcriptomic analysis and real-time PCR (RT-PCR).

METHOD DETAILS

Clinical study follow-up and assessment of clinical outcome

Safety assessment was conducted by reports of adverse events following implantation of the HA molds, as well as following auricular/finger reconstructive surgery. Clinical outcome and feasibility were assessed on three factors: the regeneration of the respective constructs within the HA molds, the reconstructive surgeries using the regenerated constructs and the long-term anatomical and functional stabilities of the reconstructed ears and MP joint. For auricular reconstructions, follow-up was initiated following stage 2 of the auricular reconstructive surgery, and continued for over five years. Patients were examined at 1, 6, and 12 months after elevation surgery to monitor for swelling, inflammation, and shape of the reconstructed ear. After 12 months, patients were followed up annually to assess the structural stability of the reconstructed ears.

For MP joint reconstruction, follow-up was initiated after surgery and continued for one year. The patient was examined at 6 and 12 months to monitor for swelling, inflammation and function of the reconstructed MP joint. Functional evaluation of the third metacarpophalangeal joint includes two aspects: range of joint motion and joint grip strength. For the range of joint motion, the third metacarpal bone was immobilized and the maximum angle of movement of the third proximal phalanx was measured using a goniometer. The fulcrum of the goniometer was placed at the midpoint of the third metacarpophalangeal joint. The stationary arm of the goniometer was placed on the dorsal midline of the metacarpophalangeal bone. The moving arm was placed close to the dorsal midline of the phalangeal bone. The maximum angle of movement of the third proximal phalanx was measured. For joint grip measurement, the third metacarpophalangeal joint is flexed at a right angle, and the maximum load-bearing weight was measured using a gripper. The mean of three independent measurements was recorded.

Ear and finger-shaped chamber fabrication

Microtia patients underwent 3D CT scans of the head to acquire surface image data of their healthy contralateral ears. Similarly, our patient to undergo MP joint reconstruction also had 3D CT scans of the healthy contralateral hand. 3D digital mirror images were created using a CAD system, and these were used to print model auricles and MP joint bones by a CAM system (Spectrum 510, Z Corporation). A mold was created by casting the models in HA (Beierkang, Shanghai, China), as previously described.[11]

Metacarpophalangeal joint bones construct regeneration

The 6th and 7th costal bones were marked on the patient preoperatively. The 6th and 7th periosteum and perichondral junctions were exposed and a sharp incision was created on the ribs and costal cartilage. The periosteum and perichondrium were peeled away, and the 6th and 7th rib and costal cartilages were removed. The periosteum and perichondrium were sutured together into a large flap. The MP joint molds were sutured onto the flap, with the articular end on the perichondral section of the flap and the bone end on the periosteal section. The removed rib and costal cartilage were implanted in the subcutaneous tissue. Approximately six months following mold implantation, the regenerated finger constructs were explanted using the original incision site. The removed rib and costal cartilages were also replanted following explantation of the MP joint constructs.

Auricle construct regeneration

The 6th, 7th, and/or 8th costal cartilage on the right thorax was marked preoperatively. A skin incision oriented parallel to the costal cartilage was made, and the costal cartilage were exposed. To avoid damage to the cambium layer of the perichondrium, a sharp incision was created on the top of the ribs, and the perichondrium was peeled away from the costal cartilage. The 6th to 8th costal cartilages perichondria were sutured to form a large interconnected perichondral flap. Next, the opening of the auricle HA mold was covered and sutured to the cambial surface of the perichondral flap (Figure S3). Approximately six months following mold implantation, the regenerated auricular constructs were explanted using the original incision site. The HA mold was peeled away from the auricular construct together with the perichondrium. The removed costal cartilage was replanted *in situ* after explantation of the auricle cartilaginous construct.

Metacarpophalangeal joint reconstructive surgery

An S-shaped incision was made at the skin of the MP joint on the back of the hand to fully loosen the scar tissue at the joint capsule. During the surgery, it was found that the articular surface of the proximal MP joint was scarred and uneven, while the distal MP joint head and phalangeal bone was intact. The patient's metacarpal bone was cut 1.5 cm from the proximal MP joint, and the regenerated proximal MP joint head was implanted. The patient's metacarpal bone and the regenerated MP joint head were fixed in position by a T-shaped steel plate. The joint capsule was completely sutured, and the subcutaneous and skin tissues were closed layer by layer. Since the patient's distal MP joint head and phalangeal bone was intact, it was decided that it would not be reconstructed. The regenerated distal MP joint head was used instead for histological and biomechanical testing.

Auricular reconstructive surgery

Auricular reconstructions were conducted using Nagata's two-stage procedure, comprising construct implantation and construct elevation.[14] **Stage I**: Cartilage construct implantation - A clean and well-perfused retroauricular pocket was first created via a W-shaped or U-shaped incision in the mastoid region. The trimmed auricle cartilaginous construct was inserted into the pocket and positioned. The superior section of this framework was covered with the retroauricular skin flap and the inferior section was covered with the transposed remnant ear tissue. Two negative-pressure drainage tubes were placed in the reconstructed ear, positioned on the anterior and posterior sides of the skin flap, respectively. Application of suction removes fluid between the auricular construct and skin flap, resulting in a tight attachment of the skin flap onto the auricular construct. The suction system was removed 7 days after the surgery. **Stage II**: Auricular construct elevation - Six months after the implantation of the cartilaginous construct, the reconstructed ear was elevated on the superficial layer of the retroauricular fascia via an incision along the helix of the refabricated construct. The reconstructed ear was also fixed to the mastoid surface to generate an appropriate cephaloauricular angle. The postauricular surface of the reconstructed ear was covered with the retroauricular fascial flap. A negative-pressure drainage tube was placed under the retroauricular fascial flap and the postauricular surface of the fascia-covered construct was covered with a full-thickness skin graft acquired from the hypogastric area. The skin was sutured in place to the mastoid skin with 5-0 chromic catgut sutures.

Histology analysis

Biopsies of regenerated human bone, cartilage, and their transition zone were collected and processed. Sections of 5 mm were made and 20 slices randomly chosen from each sample for staining with H&E and Alcian blue to examine chondrogenesis and osteogenesis. Under a light microscope (Olympus, Japan), 10 fields were randomly chosen from each slice for software-based analysis (Origin 8.0, MA, USA). Immunohistochemical assessment of chondrogenesis was performed using anti-collagen II (Col II, 1:100) antibodies (Abcam, Cambridge, UK). All of the antibodies were incubated overnight at 4°C with the DBA coloration (Abcam, Cambridge, UK). For swine tissue, perichondrium tissues of the experimental and control sides were carefully harvested. Then, tissue specimens were immersed with 4% paraformaldehyde for 12h and embedded in paraffin blocks. Serial sections of 5μm were prepared with a microtome (SM2500E; Leica Microsystems, Wetzlar, Germany). Next, the samples were stained with Mayer's hematoxylin and eosin (Beyotime, China), immunohistochemical staining or Masson staining (SBJ-0290, Sen Bei Jia Biological Technology, Nanjing, China). Microscopic observations were performed using a Nikon Eclipse E800 microscope (Nikon, Melville, NY).

Immunoblotting

Proteins were extracted using RIPA buffer containing protease inhibitors. Protein samples were separated using SDS-PAGE and immunoblotting using the following primary antibodies: anti-cxcl 8 (1:1000; Abcam), anti-aggrecan (1:2000), anti-sox9 (1:2000), anti-collagen II (1:5000), and anti-RPL4 (1:1000). Then, the membranes were incubated with secondary antibodies (1:1000; all from Cell Signaling Technology). The protein bands were visualized using enhanced chemiluminescence detection kit (Millipore).

RNA extraction

Samples were snap frozen in liquid nitrogen. Total RNA was isolated using Trizol Reagent (Invitrogen Life Technologies). The concentration, purity and integrity of the exacted RNA was assessed with a NanoDrop spectrophotometer (Thermo Scientific). Sequencing libraries were constructed using the AMPure XP system (Beckman Coulter, Beverly, CA, USA), and quantified using a Bioanalyzer 2100 system (Agilent). The generated sequencing library was Paired-End (PE) sequenced on NovaSeq 6000 platform (Illumina) at Shanghai Personal Biotechnology Cp. Ltd. The original data (Raw Data) was first filtered using Cutadapt (v1.15) software to get high-quality clean data, then mapped to the reference genome of Sus scrofa using HISAT2 v2.0.5. The mapping results were used for further differential expression analysis (below) and Gene ontology (GO) analysis.

Single cell RNA sequencing

The Cell Ranger software pipeline (version 3.1.0) provided by 10×Genomics was used to demultiplex cellular barcodes, map reads to the genome and transcriptome using the STAR aligner, and down-sample reads as required to generate normalized aggregate data across samples, producing a matrix of gene counts versus cells. We processed the unique molecular identifier (UMI) count matrix using the R package Seurat (version 3.0).[42] To remove low quality cells and possible multiplet captures, which is a major concern in microdroplet-based experiments, we applied a criteria to filter out cells with UMI/gene numbers out of the limit of mean value +/− 2-fold of standard deviations assuming the UMI/gene numbers are Guassian distributed. Following visual inspection of the distribution of cells by the fraction of mitochondrial genes expressed, we low-quality cells (assessed using percentage of mitochondrial genes) were discarded. Library size normalization was performed in Seurat on the filtered matrix to obtain the normalized count.

Top variable genes across single cells were identified using methods previously described.[43] Briefly, the average expression and dispersion were calculated for each gene, which were subsequently binned based on expression. Principal component analysis (PCA) was performed to reduce the dimensionality on the log transformed gene-barcode matrices of top variable genes. A graph-based was used for clustering cells, which were subsequently visualized in 2-dimension using tSNE. A likelihood ratio test that simultaneously test for changes in mean expression and in the percentage of expressed cells was used to identify significant differentially expressed genes between clusters. Here, we use the R package SingleR,[44] a novel computational method for unbiased cell type recognition of scRNA-seq to infer the cell of origin of each of the single cells independently and identify cell types.

Differentially expressed genes (DEGs) were identified using the Seurat package. p value <0.05 and |log2foldchange| > 1 (or |log2foldchange| > 0.58) was set as the threshold for significantly differential expression. GO enrichment and KEGG pathway enrichment analysis of DEGs were respectively performed using R based on the hypergeometric distribution.

Statistical analysis

Numerical data are provided as mean ± S.E.M., and median (range) for categorical data. Pairwise statistical analyses were performed using the t-test, or the Mann-Whitney U-test for categorical variables. Statistical analyses involving three or more groups were evaluated using the one-way ANOVA. Subsequent pairwise comparisons were performed with a Bonferroni's *post-hoc* correction for multiple comparisons. p-values of less than 0.05 were considered statistically significant. Statistical analyses were performed using Graph Pad Prism 5.2 (GraphPad Software, San Diego, CA, USA). Gene expression data were presented as candle plots.